Gradient Schemes for Image Processing

Robert Eymard, Angela Handlovičová , Raphaèle Herbin, Karol Mikula and Olga Stašová

Abstract We present a gradient scheme (which happens to be similar to the MPFA finite volume O-scheme) for the approximation to the solution of the Perona-Malik model regularized by a time delay and to the solution of the nonlinear tensor anisotropic diffusion equation. Numerical examples showing properties of the method and applications in image filtering are discussed.

Key words: advection equation, semi-implicit scheme, finite volume method
MSC2010: 35L04, 65M08, 65M12

1 Introduction

A series of methods for image processing are based on the use of approximate solutions to equations of the type

$$u_t - \text{div } (G(u,x,t)\nabla u) = r(x,t), \text{ for a.e. } (x,t) \in \Omega \times]0,T[\tag{1}$$

with the initial condition

$$u(x,0) = u_{\text{ini}}(x), \text{ for a.e. } x \in \Omega, \tag{2}$$

Robert Eymard,
Université Paris-Est, 5 boulevard Descartes Champs-sur-Marne F-77454 Marne la Vallée, France, e-mail: robert.eymard@univ-mlv.fr

Raphaèle Herbin
Centre de Mathmatiques et Informatique, Université de Provence, 39 rue Joliot Curie, 13453 Marseille 13, France, e-mail: raphaele.herbin@cmi.univ-mrs.fr

Angela Handlovičová, Karol Mikula, Olga Stašová
Department of Mathematics, Slovak University of Technology, Radlinského 11, 81368 Bratislava, Slovakia, e-mail: angela@math.sk, mikula@math.sk, stasova@math.sk

and the homogeneous Neumann boundary condition

$$G(u,x,t)\nabla u(x,t)\cdot \mathbf{n}_{\partial\Omega}(x) = 0, \text{ for a.e. } (x,t)\in \partial\Omega\times\mathbb{R}_+, \tag{3}$$

where Ω is an open bounded polyhedron in $\mathbb{R}^d$, $d\in\mathbb{N}^\star$, with boundary $\partial\Omega$, $T>0$, $u_{\rm ini}\in L^2(\Omega)$, $r\in L^2(\Omega\times]0,T[)$, and G is such that, for all $v\in L^2(\Omega)$ and a.e. $(x,t)\in\Omega\times]0,T[$, $G(v,x,t)$ is a self-adjoint linear operator with eigenvalues in $(\underline{\lambda},\overline{\lambda})$ with $0<\underline{\lambda}\le\overline{\lambda}$, and $G(v,x,t)$ is continuous with respect to v and measurable with respect to x,t. In image processing applications, $u_{\rm ini}$ represents an original noisy image, the solution $u(x,t)$ represents its filtering which depends on scale parameter t and $d=2$ for $2D$ image filtering, $d=3$ for $3D$ image or $2D$+time movie filtering and $d=4$ for $3D$+time filtering of spatio-temporal image sequences.

The image processing methods based on approximations of equation (1) differ by definition of the function G. The first such model was proposed by Perona-Malik in 1987 [9], and nowadays, its regularization (by spatial convolution) due to Catte, Lions, Morel and Coll [2] is usually used. The regularized equation has the following form

$$\partial_t u - \nabla.(g(|\nabla G_\sigma * u|)\nabla u) = 0 \tag{4}$$

where $g(s)$ is a Lipschitz continuous decreasing function, $g(0)=1$, $0<g(s)\to 0$ for $s\to\infty$, $G_\sigma\in C^\infty(\mathbb{R}^d)$ is a smoothing kernel, e.g. the Gauss function or mollifier with a compact support, for which $\int_{\mathbb{R}^d} G_\sigma(x)dx = 1$. Thanks to convolution, the nonlinearity in difusion term depends on the unknown function u, opposite to the original Perona-Malik equation (without convolution) where it depends on the gradient of solution. For the regularized model, the finite volume scheme were suggested and convergence and error estimates were proved in [8], [3].

Next interesting image processing model with the structure of equation (1) is the so-called nonlinear tensor anisotropic diffusion introduced by Weickert [11]. In that case, the matrix $G(u,x,t)$ represents the so-called diffusion tensor depending on the eigenvalues and eigenvectors of the (regularized) structure tensor

$$J_\rho(\nabla u_{\tilde\imath}) = G_\rho * (\nabla u_{\tilde\imath}\nabla u_{\tilde\imath}{}^T), \tag{5}$$

where

$$u_{\tilde\imath}(x,t) = (G_{\tilde\imath} * u(\cdot,t))(x) \tag{6}$$

and $G_{\tilde\imath}$ and G_ρ are Gaussian kernels. In computer vision, the matrix $J_\rho = \begin{pmatrix} a & b \\ b & c \end{pmatrix}$, which is symmetric and positive semidefinite, is also known as the interest operator or second moment matrix. If we denote $x=(x_2,x_2)$ we can write $a = G_\rho * \left(\frac{\partial G_{\tilde\imath}}{\partial x_1} * u\right)^2$, $b = G_\rho * \left(\left(\frac{\partial G_{\tilde\imath}}{\partial x_1} * u\right)\left(\frac{\partial G_{\tilde\imath}}{\partial x_2} * u\right)\right)$ and $c = G_\rho * \left(\frac{\partial G_{\tilde\imath}}{\partial x_2} * u\right)^2$. The orthogonal set of eigenvectors (v,w) of J_ρ corresponding to its eigenvalues (μ_1,μ_2), $\mu_1\ge\mu_2$, is such that the orientation of the eigenvector w, which corresponds to the smaller eigenvalue μ_2, gives the so-called coherence orientation. This orientation has the lowest fluctuations in image intensity. The diffusion tensor G in equation

(1) is then designed to steer a smoothing process such that the filtering is strong along the coherence direction w and increasing with the coherence defined by difference of eigenvalues $(\mu_1-\mu_2)^2$. To that goal, G must possess the same eigenvectors $v=(v_1,v_2)$ and $w=(-v_2,v_1)$ as the structure tensor $J_\rho(\nabla u_{\bar{t}})$ and the eigenvalues of G can be chosen as follows

$$\begin{aligned} &\kappa_1 = \alpha, \quad \alpha \in (0,1),\ \alpha \ll 1, \\ &\kappa_2 = \begin{cases} \alpha, & \text{if } \mu_1=\mu_2, \\ \alpha+(1-\alpha)\exp\left(\frac{-C}{(\mu_1-\mu_2)^2}\right),\ C>0 & \text{else.} \end{cases} \end{aligned} \tag{7}$$

So, the matrix G is finally defined by

$$G = ABA^{-1}, \quad \text{where} \quad A=\begin{pmatrix} v_1 & -v_2 \\ v_2 & v_1 \end{pmatrix} \quad \text{and} \quad B=\begin{pmatrix} \kappa_1 & 0 \\ 0 & \kappa_2 \end{pmatrix}. \tag{8}$$

By the construction, again thanks to convolutions, we see that diffusion matrix depends nonlinearly on the solution u and it satisfies smoothness, symmetry and uniform positive definitness properties. The so-called diamond-cell finite volume schemes for the nonlinear tensor anisotropic diffusion were suggested and analyzed in [6, 7].

In this paper, we use a new class of finite volume schemes, the so-called gradient schemes [5], for solving image processing models based on equation (1). Moreover, we suggest and study numerically new type of regularization of the classical Perona-Malik approach by considering the gradient information from delayed time $t-\bar{t}$. We called this model time-delayed Perona-Malik equation, and consider (1) with $u_{\text{ini}} \in H^1(\Omega)$, and we define $u(x,t)=u_{\text{ini}}(x)$ for $x \in \Omega$ and $t<0$ and function G is defined by

$$G(u,x,t) = \max\left(\frac{1}{1+|\nabla u(x,t-\bar{t})|^2}, \alpha\right) \tag{9}$$

where $\bar{t}$ is a time delay and $\alpha>0$ is a parameter. It turns out that for any $k \in \mathbb{N}$ in the time interval $]k\bar{t},(k+1)\bar{t}[$, G is a given function of (x,t) only, which leads to a construction of efficient linear numerical scheme for this type of problems.

2 Gradient scheme approximation

In order to describe the scheme, we now introduce some notations for the space discretisation.

1. A rectangular discretisation of Ω is defined by the increasing sequences $a_i = x_0^{(i)} < x_1^{(i)} < \ldots < x_{n^{(i)}}^{(i)} = b_i$, $i=1,\ldots,d$.
2. We denote by

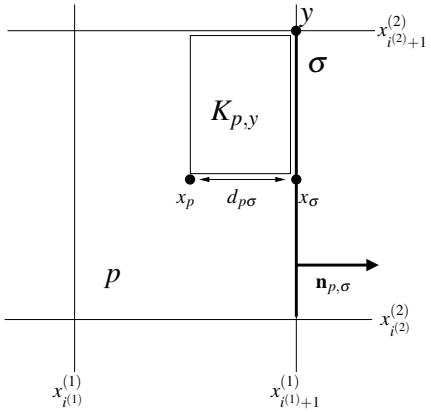

Fig. 1 Notations for the meshes

$$\mathscr{M} = \left\{]x^{(1)}_{i^{(1)}}, x^{(1)}_{i^{(1)}+1}[\times \ldots \times]x^{(d)}_{i^{(d)}}, x^{(d)}_{i^{(d)}+1}[,\ 0 \le i^{(1)} < n^{(1)},\ \ldots,\ 0 \le i^{(d)} < n^{(d)} \right\}$$

the set of the control volumes. The elements of $\mathscr{M}$ are denoted $p, q, \ldots$. We denote by $\boldsymbol{x}_p$ the centre of p. For any $p \in \mathscr{M}$, let $\partial p = \overline{p} \setminus p$ be the boundary of p; let $|p| > 0$ denote the measure of p and let h_p denote the diameter of p and $h_{\mathscr{D}}$ denote the maximum value of $(h_p)_{p \in \mathscr{M}}$.

3. We denote by $\mathscr{E}_p$ the set of all the faces of $p \in \mathscr{M}$, by $\mathscr{E}$ the union of all $\mathscr{E}_p$, and for all $\sigma \in \mathscr{E}$, we denote by $|\sigma|$ its $(d-1)$-dimensional measure. For any $\sigma \in \mathscr{E}$, we define the set $\mathscr{M}_\sigma = \{p \in \mathscr{M}, \sigma \in \mathscr{E}_p\}$ (which has therefore one or two elements), we denote by $\mathscr{E}_p$ the set of the faces of $p \in \mathscr{M}$ (it has $2d$ elements) and by $\boldsymbol{x}_\sigma$ the centre of σ. We then denote by $d_{p\sigma} = |\boldsymbol{x}_\sigma - \boldsymbol{x}_p|$ the orthogonal distance between $\boldsymbol{x}_p$ and $\sigma \in \mathscr{E}_p$ and by $\mathbf{n}_{p,\sigma}$ the normal vector to σ, outward to p.
4. We denote by $\mathscr{V}_p$ the set of all the vertices of $p \in \mathscr{M}$ (it has 2^d elements), by $\mathscr{V}$ the union of all $\mathscr{V}_p$, $p \in \mathscr{M}$. For $y \in \mathscr{V}_p$, we denote by $K_{p,y}$ the rectangle whose faces are parallel to those of p, and whose the set of vertices contains $\boldsymbol{x}_p$ and y. We denote by $\mathscr{V}_\sigma$ the set of all vertices of $\sigma \in \mathscr{E}$ (it has 2^{d-1} elements), and by $\mathscr{E}_{p,y}$ the set of all $\sigma \in \mathscr{E}_p$ such that $y \in \mathscr{V}_\sigma$ (it has d elements).
5. We define the set $X_{\mathscr{D}}$ of all $u = ((u_p)_{p \in \mathscr{M}}, (u_{\sigma,y})_{\sigma \in \mathscr{E}, y \in \mathscr{V}_\sigma})$, where all u_p and $u_{\sigma,y}$ are real numbers.
6. We denote, for all $u \in X_{\mathscr{D}}$, by $\Pi_{\mathscr{D}} u \in L^2(\Omega)$ the function defined by the constant value u_p a.e. in $p \in \mathscr{M}$.
7. For $u \in X_{\mathscr{D}}$, $p \in \mathscr{M}$ and $y \in \mathscr{V}_p$, we denote by

$$\nabla_{p,y} u = \frac{2}{|p|} \sum_{\sigma \in \mathscr{E}_{p,y}} |\sigma| (u_{\sigma,y} - u_p) \mathbf{n}_{p,\sigma} = \sum_{\sigma \in \mathscr{E}_{p,y}} \frac{u_{\sigma,y} - u_p}{d_{p\sigma}} \mathbf{n}_{p,\sigma}, \qquad (10)$$

and by $\nabla_{\mathscr{D}} u$ the function defined a.e. on Ω by $\nabla_{p,y} u$ on $K_{p,y}$.

Let $T>0$ be given, and $\tau>0$ such that there exists $N_T\in\mathbb{N}$ with $T=N_T\tau$, We then define $X_{\mathscr{D},\tau}=X_{\mathscr{D}}^{N_T}=\{(u^n)_{n=1,\dots,N_T},u^n\in X_{\mathscr{D}}\}$, and we define the mappings $\Pi_{\mathscr{D},\tau}:X_{\mathscr{D},\tau}\to L^2(\Omega)$ and $\nabla_{\mathscr{D},\tau}:X_{\mathscr{D},\tau}\to L^2(\Omega)^d$ by

$$\Pi_{\mathscr{D},\tau}u(x,t)=\Pi_{\mathscr{D}}u^n(x),\ \text{for a.e. } x\in\Omega,\ \forall t\in](n-1)\tau,n\tau],\ \forall n=1,\dots,N_T, \quad (11)$$

$$\nabla_{\mathscr{D},\tau}u(x,t)=\nabla_{\mathscr{D}}u^n(x),\ \text{for a.e. } x\in\Omega,\ \forall t\in](n-1)\tau,n\tau],\ \forall n=1,\dots,N_T. \quad (12)$$

We then define the following gradient scheme approximation [5] for the discretization of Problem (1):

$$\begin{aligned}&u\in X_{\mathscr{D},\tau},\ D_\tau u(x,t):=\frac{1}{\tau}(\Pi_{\mathscr{D}}u^1(x)-u_{\rm ini}(x)),\ \text{for a.e. } x\in\Omega,\ \forall t\in]0,\tau],\\&D_\tau u(x,t)=\frac{1}{\tau}(\Pi_{\mathscr{D}}u^n(x)-\Pi_{\mathscr{D}}u^{n-1}(x)),\\&\text{for a.e. } x\in\Omega,\ \forall t\in](n-1)\tau,n\tau],\forall n=2,\dots,N_T,\end{aligned} \quad (13)$$

and

$$\begin{aligned}&\int_0^T\int_\Omega\left(D_\tau u\,\Pi_{\mathscr{D},\tau}v+G_{\mathscr{D},\tau}(\Pi_{\mathscr{D},\tau}u,x,t)\nabla_{\mathscr{D},\tau}u\cdot\nabla_{\mathscr{D},\tau}v\right)\mathrm{d}x\mathrm{d}t\\&=\int_0^T\int_\Omega r\Pi_{\mathscr{D},\tau}v\mathrm{d}x\mathrm{d}t,\ \forall v\in X_{\mathscr{D},\tau},\end{aligned} \quad (14)$$

where $G_{\mathscr{D},\tau}(v,x,t)$ is a suitable approximation of $G(v,x,t)$. The mathematical properties of this scheme are studied in [4].

Remark 1. The equations obtained, for a given $y\in\mathscr{V}$, defining $v\in X_{\mathscr{D}}$ for a given $\sigma\in\mathscr{E}_y$ by $v_{\sigma,y}=1$ and all other degrees of freedom null, constitute a local invertible linear system, allowing for expressing all $(u_{\sigma,y})_{\sigma\in\mathscr{E}_y}$ with respect to all $(u_p)_{p\in\mathscr{M}}$. This leads to a nine-point stencil on rectangular meshes in 2D, 27-point stencil in 3D (this property is the basis of the MPFA O-scheme [1]).

3 Numerical experiments

3.1 Numerical study of the error for the time-delayed Perona-Malik model

We consider equation (1) in case of G defined by (9) and with a right hand side computed such that the function $u(x,y,t)=((x^2+y^2)/2-(x^3+y^3)/3)t$ is its exact solution. The domain Ω is square $[0,1]\times[0,1]$. We consider two cases, first, the time delay $\bar{t}=0.0625$ and the overal time $T=0.625$, and then $\bar{t}=0.625$ and $T=1.25$. In both cases we used coupling between space and time step $\tau\approx h^2$, where $h=\frac{1}{n}$ is length of the side of finite volume in uniform squared partition of Ω. We observe the second order convergence in L^2 and L^∞ norms of solution (denoted by E_2 and E_∞) and its gradient (denoted by EG_2 and EG_∞) in this special example, see Tables 1 and 2.

Table 1 The errors and EOC for the time-delayed Perona-Malik model, $\bar{t} = 0.0625$, $T = 0.625$.

n	τ	E_2	EOC	E_∞	EOC	EG_2	EOC	EG_∞	EOC
4	0.0625	4.771e-4	-	1.022e-3	-	7.184e-3	-	1.450e-2	-
8	0.015625	1.172e-4	1.429	2.692e-4	1.925	1.707e-3	2.073	3.615e-3	2.004
16	0.00390625	2.913e-5	2.604	6.812e-5	1.982	4.213e-4	2.019	9.031e-4	2.001
32	0.0009765625	7.270e-6	2.002	1.708e-5	1.996	1.050e-4	2.004	2.257e-4	2.000
64	0.000244140625	1.815e-6	2.001	4.273e-6	1.999	2.624e-5	2.000	5.643e-5	1.999

Table 2 The errors and EOC for the time-delayed Perona-Malik model, $\bar{t} = 0.625$, $T = 1.25$.

n	τ	E_2	EOC	E_∞	EOC	EG_2	EOC	EG_∞	EOC
4	0.0625	1.482e-3	-	2.237e-3	-	1.913e-2	-	2.848e-2	-
8	0.015625	3.745e-4	1.985	5.889e-4	1.925	4.651e-3	2.040	7.083e-3	2.007
16	0.00390625	9.379e-5	1.998	1.450e-4	2.022	1.155e-3	2.009	1.768e-3	2.002
32	0.0009765625	2.346e-5	1.999	3.735e-5	1.957	2.881e-4	2.003	4.419e-4	2.000
64	0.000244140625	5.865e-6	2.000	9.343e-6	1.999	7.201e-5	2.003	1.105e-4	2.000

3.2 Image filtering by the time-delayed Perona-Malik model

The example of image filtering by the gradient scheme applied to the time-delayed Perona-Malik equation is presented in Figure 2. The original clean image can be seen in Figure 2 left top. It is damaged by 40% additive noise, see Figure 2 right top. In the bottom raws of Figure 2 we present 5th, 10th and 20th denoising step which show the reconstruction of the original. In the last step we see the correct shape reconstruction with the keeping of the edge, with only slighly changed intensity values inside and outside quatrefoil due to diffusion. The following parameters were used in computations: $n^{(1)} = n^{(2)} = 200,\ h = 0.0125, \tau = 0.01, \bar{t} = 0.1$.

3.3 Image filtering by the nonlinear anisotropic tensor diffusion

In this example we present the image denoising by the nonlinear tensor diffusion and show improvement of the coherence of the line structures, which is the basic property of such models. Here, in the evaluation of diffusion matrix we use the semi-implicit approach, which means that in (6) we use the solution shifted by one time step backward, $u_{\bar{t}}(x,t) = (G_{\bar{t}} * u(\cdot, t-\tau))(x)$, cf. also [6]. The original image with three crackling lines can be seen in Figure 3 left. On the right, one can see its filtering after 100 time steps which indeed enhance the coherence of those line structures. In this experiment we used the following parameters: $n^{(1)} = n^{(2)} = 250$, $h = 0.01$, $\tau = 0.0001$, $\tilde{t} = 0.0001$, $\rho = 0.01$, $\alpha = 0.001$, $C = 1$.

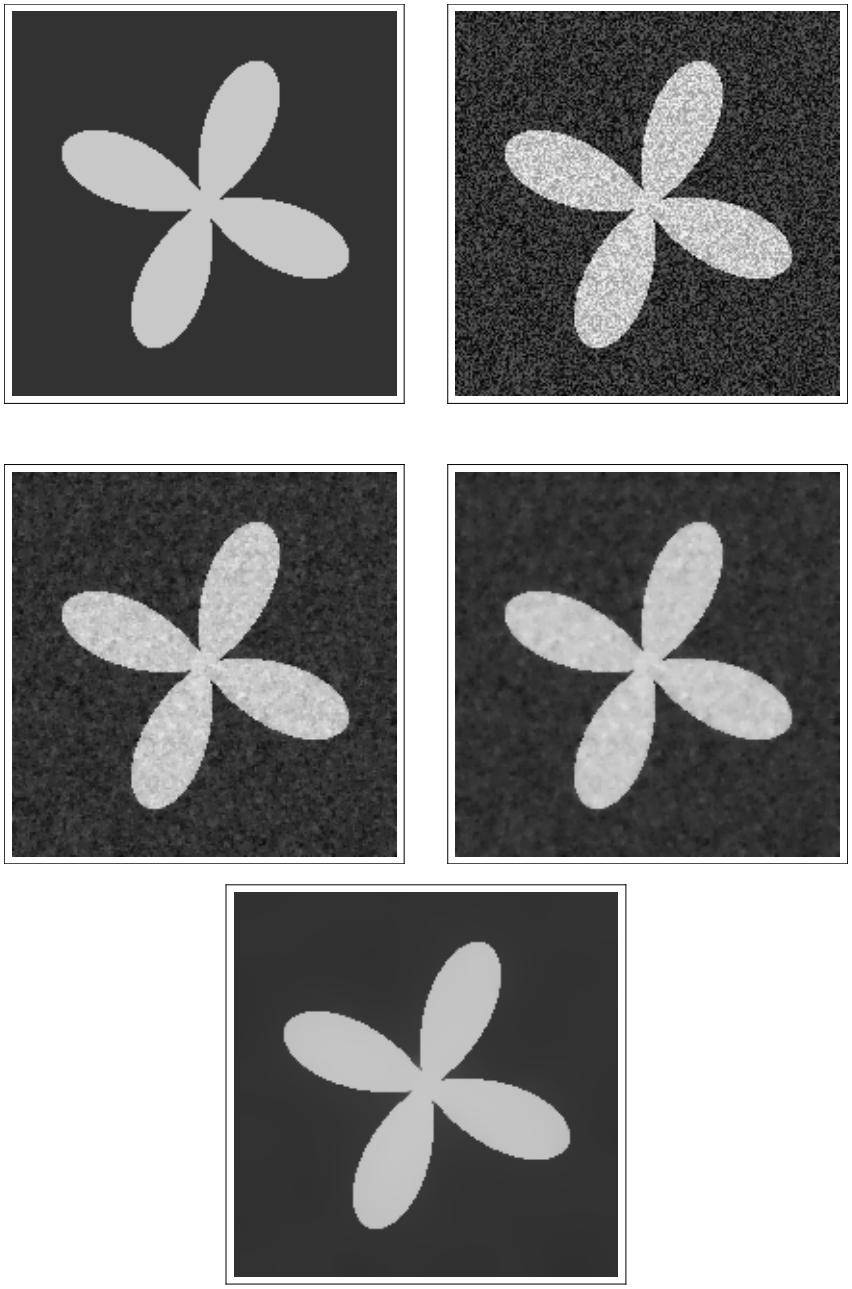

Fig. 2 Image filtering by the time-delayed Perona-Malik model: the original image (left top), the noisy image (right top) and the results after 5, 10 and 20 filtering steps.

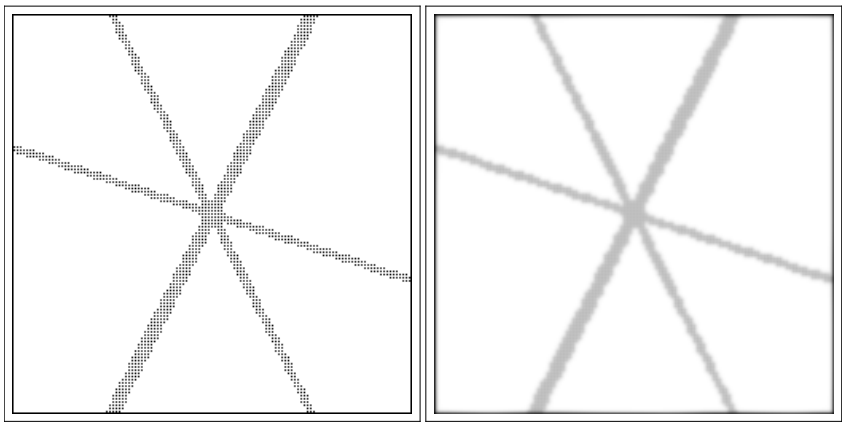

Fig. 3 The enhancement of the coherence by the nonlinear anisotropic tensor diffusion, original image (left) and the result of filtering after 100 time steps (right).

References

1. I. Aavatsmark, T. Barkve, O. Boe, and T. Mannseth. Discretization on non-orthogonal, quadrilateral grids for inhomogeneous, anisotropic media. *J. Comput. Phys.*, 127(1):2–14, 1996.
2. F. Catté, P.L. Lions, J.M. Morel and T. Coll. Image selective smoothing and edge detection by nonlinear diffusion. *SIAM J. Numer. Anal.* 29:182–193,1992.
3. A. Handlovičová and Z. Krivá. Error estimates for finite volume scheme for Perona - Malik equation. *Acta Math. Univ. Comenianae*,74,(1):79–94, 2005.
4. R. Eymard, A. Handlovičová, R. Herbin, K. Mikula and O. Stašová. Applications of approximate gradient schemes for nonlinear parabolic equations. *in preparation*, 2011.
5. R. Eymard, R. Herbin. Gradient Scheme Approximations for Diffusion Problems. *these proceedings*, 2011.
6. O. Drblíková and K. Mikula. Convergence Analysis of Finite Volume Scheme for Nonlinear Tensor Anisotropic Diffusion in Image Processing. *SIAM Journal on Numerical Analysis*, 46 (1): 37–60,2007.
7. O. Drblíková A. Handlovičová and K. Mikula. Error estimates of the Finite Volume Scheme for the Nonlinear Tensor -Driven Anisotropic Diffusion. *Applied Numerical Mathemtaics*, 59: 2548–2570,2009.
8. K. Mikula and N. Ramarosy. Semi-implicit finite volume scheme for solving nonlinear diffusion equations in image processing. *Numerische Mathematik*,89, (3):561–590,2001.
9. P. Perona, J. Malik. Scale space and edge detection using anisotropic diffusion. In: Proc. IEEE Computer Society Workshop on Computer Vision (1987)
10. N. J. Walkington. Algorithms for computing motion by mean curvature. *SIAM J. Numer. Anal.*, 33(6):2215–2238, 1996.
11. J. Weickert. Coherence-enhancing diffusion filtering. *Int. J. Comput. Vision*, 31: 111–127,1999.

The paper is in final form and no similar paper has been or is being submitted elsewhere.